
Article:
Varnava, Christian, Stevenson, R. Mark, Nilsson, Jonas et al. (2016) An entangled-LED-driven quantum relay over 1km. npj Quantum Information. 16006. ISSN: 2056-6387

https://doi.org/10.1038/npjqi.2016.6

---

npj | Quantum Information

www.nature.com/npjqi

ARTICLE OPEN

An entangled-LED-driven quantum relay over 1 km

Christiana Varnava[1,2], R Mark Stevenson[1], Jonas Nilsson[1], Joanna Skiba-Szymanska[1], Branislav Dzurňák[1,4], Marco Lucamarini[1], Richard V Penty[2], Ian Farrer[3,5], David A Ritchie[3] and Andrew J Shields[1]

Quantum cryptography allows confidential information to be communicated between two parties, with secrecy guaranteed by the laws of nature alone. However, upholding guaranteed secrecy over networks poses a further challenge, as classical receive-and-resend routing nodes can only be used conditional of trust by the communicating parties, which arguably diminishes the value of the underlying quantum cryptography. Quantum relays offer a potential solution by teleporting qubits from a sender to a receiver, without demanding additional trust from end users. Here we demonstrate the operation of a quantum relay over 1 km of optical fibre, which teleports a sequence of photonic quantum bits to a receiver by utilising entangled photons emitted by a semiconductor light-emitting diode. The average relay fidelity of the link is 0.90 ± 0.03, exceeding the classical bound of 0.75 for the set of states used, and sufficiently high to allow error correction. The fundamentally low multiphoton emission statistics and the integration potential of the source present an appealing platform for future quantum networks.

npj Quantum Information (2016) **2,** 16006; doi:10.1038/npjqi.2016.6; published online 15 March 2016

INTRODUCTION

Quantum key distribution[1,2] systems based on weak-coherent optical pulses have been reported that allow unique cryptographic keys to be shared between directly connected users on point-to-point[3–5] or point-to-multipoint links[6]. To establish fully quantum multipartite networks, that avoid trusting intermediate parties,[7] it is necessary to route quantum signals through a backbone of quantum nodes.[8] This can be achieved by leveraging quantum entanglement to set-up non-local correlations between measurements by end users. Examples of such schemes are distribution of entangled photon pairs to end users, where local measurements are performed,[9] or conversely, where photons are sent by two users to be projected into a Bell state by an intermediate quantum node.[10–12] Photonic quantum repeaters[13] and relays[8] use both of these effects to teleport entangled or single qubits, respectively, in a manner that can be chained to create a fully quantum network for which theoretically proven quantum security can be preserved.

Here we report operation of a quantum relay over 1 km of optical fibre using entangled photons generated by a light-emitting diode to teleport photonic qubits encoded on weak coherent pulses emitted by a laser. Compared with previously reported quantum relays[14] and photonic teleportation over significant distances,[15,16] our system is directly electrically driven using a simple semiconductor device, offering a route to large-scale network deployments. Teleporting weak coherent states offers potential enhancements to state-of-the art quantum key distribution systems, as it creates output photons with sub-Poissonian statistics immune to the photon number-splitting attack,[17,18] and protects against intrusions.[19]

RESULTS

At the heart of our quantum relay is an entangled-light-emitting diode (ELED),[20] as shown in Figure 1a. It consists of a layer of self-assembled indium arsenide quantum dots within a gallium arsenide microcavity (Materials and Methods). We have optimised the resistance and capacitance of the device to allow it to be driven by short electrical pulses, without compromising entanglement fidelity or photon coherence. This has allowed electrically triggered quantum teleportation using a light-emitting diode, which has previously been limited to only direct current operation.[18,21]

An image of the ELED in operation is shown in Figure 1b. Individual points of light are observed, corresponding to light emission from individual quantum dots. We select emission from a chosen quantum dot, indicated in the inset image, by collection with a single-mode fibre. The emission spectrum measured by a grating spectrometer and charge-coupled device camera is shown in Figure 1c. Two strong emission lines are observed corresponding to the first, biexciton photon (*B*) and second, exciton photon (*X*) emission. The *B* and *X* emission lines are then spectrally filtered with a diffraction grating to isolate them from each other and other emission from the device, including that originating from the quantum well-like wetting layer, and any other nearby quantum dots (such as the weak peak seen at ~888 nm).

The ELED was driven at a repetition rate of 203 MHz, with pulses of nominally 0.4 V amplitude and 490 ps duration. Time-resolved electroluminescence was measured under these conditions and shown in Figure 1d for *B* as a black line. The emission is strongly pulsed, and well contained within each cycle.

The experimental quantum relay system is shown in Figure 2a. It comprises four sections separated by three 350-m fibre-optic links. The first 'sender' section is thus separated from the last 'receiver' section by 1.05 km of optical fibre. Entangled photons emitted by the ELED are divided, the *B* photons are sent to the Bell-state measurement (BSM) section and the *X* photons are sent to the receiver. The sender uses a wavelength-tunable continuous-wave laser diode, from which pulses are generated by an external

[1]Toshiba Research Europe Limited, Cambridge, UK; [2]Electrical Division, Department of Engineering, University of Cambridge, Cambridge, UK and [3]Cavendish Laboratory, University of Cambridge, Cambridge, UK.
Correspondence: RM Stevenson (mark.stevenson@crl.toshiba.co.uk)
[4]Current address: Department of Physics and Astronomy, University of Sheffield, Sheffield, UK
[5]Current address: Department of Electronic and Electrical Engineering, University of Sheffield, Sheffield, UK
Received 5 October 2015; revised 21 January 2016; accepted 27 January 2016

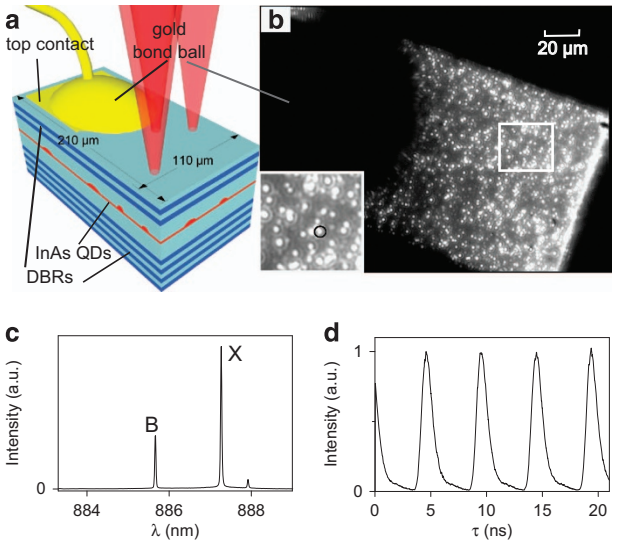

Figure 1. ELED. (**a**) Schematic of the ELED used in this experiment (not to scale). The entangled photon source is an InAs quantum dot (QD) embedded in a p–i–n diode structure with a cavity centred at 886 nm, between top and bottom distributed Bragg reflectors (DBRs). (**b**) Microscope image of the mesa used for this experiment. Individual quantum dots can be identified as points of light in the image. The dark circular area is the gold bond to the top contact. The quantum dot chosen for the experiment is identified in the inset. (**c**) Biexciton (*B*) and exciton (*X*) electroluminescence spectrum under experimental biasing conditions. (**d**) Time-resolved biexciton electroluminescence.

optical intensity modulator, tuned to the frequency of the ELED. The polarised pulses are then rotated by a polarisation controller PC1 to encode the qubit, before transmission to the 'BSM' section.

At the 'BSM' section, an imbalanced beamsplitter BS combines 95% of the *B* photons, with 5% of the laser photons into one output arm, before a polarisation controller PC2 and polarising beamsplitter projects horizontal (*H*) and vertical (*V*) polarised photons onto superconducting single-photon detectors D1 and D2. The function of this section is to perform a BSM in the state $(|H_L V_B\rangle + |V_L H_B\rangle)/\sqrt{2}$, where subscripts *L* and *B* denote photons originating from the laser and biexciton, respectively. Such a measurement collapses the formerly entangled *X* photon into a quantum state related to the input qubit, together with a trivial unitary transformation.[22] In this work, input qubits of the form $\cos(a)|H_L\rangle + e^{ib}\sin(a)|V_L\rangle$ are teleported to the state $\cos(a)|V_X\rangle + e^{ib}\sin(a)|H_X\rangle$.

Theoretical analysis of the intricate time-dependent three-photon fields reveals a range of laser pulse conditions for which the calculated peak teleportation fidelities are close to optimum (Materials and Methods). The laser pulse properties observed at detectors D1 and D2 were set accordingly, with integrated intensity of 0.85 relative to the *B* pulse, a fitted Gaussian full width at half maximum of 0.95 ± 0.01 ns and a delay of the laser pulse after the *B* pulse of 0.60 ± 0.02 ns relative to maximum overlap.

The entanglement properties of the photons emitted by the ELED were characterised within the quantum relay system. Second-order correlation measurements were performed in the rectilinear {*H*, *V*} and diagonal {*D*, *A*} linear polarisation bases, where *D* and *A* represent the diagonal and anti-diagonal polarisations, respectively. From these measurements it is possible to determine Bell's parameter to indicate the degree of entanglement present.[23] The result is shown in Figure 2b as a function of the time delay τ_{BX} between a biexciton photon detected at D1 or D2, and an exciton photon at D3 or D4. For simultaneously detected photons, a Bell parameter of 2.59 ± 0.01 is observed, exceeding the limit of 2 for classical behaviour, and corresponding to 91.8% of the ideal value of $2\sqrt{2}$. To our knowledge, this is the first time entanglement has been distributed by a quantum dot source over a distance longer than a few metres.

The quantum relay was operated using polarisation-encoded BB84 quantum states,[24] using the rectilinear and diagonal bases. Three-photon detection statistics were recorded between a pair of photons at D1 and D2, and one at D3 or D4. The polarisations of the input qubit and measurement basis, controlled by PC1 and PC3, respectively, were switched during the experiment so that a randomised sequence of teleported qubits could be recorded.

Figure 2c shows the measured third-order correlation function $g^{(3)}$ averaged over all four polarisation inputs, and over the corresponding co- and cross-polarised outputs. The horizontal and vertical axes are the time delays τ_2 and τ_3 between photon detection at D1 or D2, respectively, and a photon at D3 or D4. The intensity distribution has highly pulsed character, with peaks occurring when the delays τ_2 and τ_3 are an integer multiple of the 4.9 ns repetition period. This is in contrast to previous reports of quantum teleportation with quantum dots, which operated in continuous mode. Stronger intensity peaks are observed for $\tau_2 = 0$ and $\tau_3 = 0$, as exciton emission directly following biexciton emission is enhanced. For coincident detection at D1 and D2, $\tau_2 = \tau_3$, a low-intensity line indicates a suppression in detecting two *B* photons simultaneously due to the sub-Poissonian nature of the ELED source.

The polarisation dependence of the quantum relay is evaluated from the difference between third-order correlation measurements with the expected, and unexpected (i.e., orthogonal to expected) output polarisations. Such $g^{(3)}$ contrast measurements are presented in Figure 3 as a function of τ_2 and τ_3 for each of the input qubit states *H*, *V*, *D* and *A*. High contrast at $\tau_2 = 0$ ($\tau_3 = 0$) is observed due to *H* (*V*) input laser photons exciting the D1 (D2) detector, so that contrast is dominated by correlation between *X* and a *B* photon at D2 (D1). The correlation contrast for *D* and *A* however looks quite different, dominated by a peak centred at $\tau_3 = \tau_2 = 0$, as two-photon interference between simultaneously detected photons is required for teleporting states in a superposition state. Calculations, shown in the right column, agree well with observations (Materials and Methods).

The performance of the quantum relay is assessed by determining the relay fidelity F_P, which for each input photon state *P* is determined by:

$$F_P(\tau_3, \tau_2) = g^{(3)}_{P'}(\tau_3, \tau_2)/(g^{(3)}_{P'}(\tau_3, \tau_2) + g^{(3)}_{Q'}(\tau_3, \tau_2)),$$

where P' and Q' are the expected and orthogonal unexpected output polarisations, respectively. Averaging across the four input states *H*, *V*, *D* and *A* gives the average relay fidelity *F*, which is plotted in Figure 4a. A clear peak is observed around $\tau_2 = \tau_3 = 0$, where the fidelity clearly exceeds 0.75, the limit for optimal classical teleportation scheme for this four-state protocol (Materials and Methods). Calculated behaviour, shown in Figure 4b, shows similar features. The maximum measured value of *F* is more clearly observed in Figure 4c, which plots *F* as a function of τ_2 or τ_3 for simultaneous detection of two photons at the 'BSM' section. The peak rises to a maximum value of 0.900 ± 0.028, exceeding the six-state average fidelity reported previously.[18] The corresponding measured individual relay fidelities are 0.957 ± 0.042 and 0.951 ± 0.0475 from polar states *H* and *V*, and 0.845 ± 0.064 and 0.847 ± 0.063 for superposition states *D* and *A*, respectively.

The high measured teleportation fidelities confirm that sender and receiver have shared information in excess of any information held by an eavesdropper. The difference between unity and the

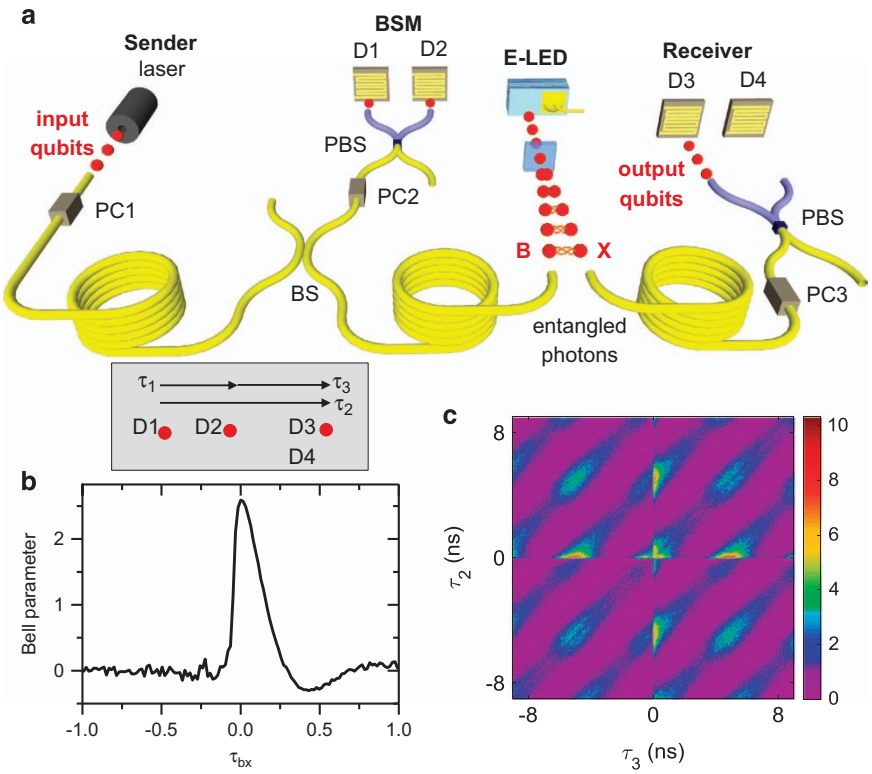

Figure 2. Quantum relay experimental set-up. (**a**) The sender encodes photons from an externally modulated laser diode with qubit states $|H\rangle$, $|V\rangle$, $|D\rangle$ and $|A\rangle$, using a polarisation controller PC1, to be transferred to the receiver by quantum teleportation. Sender and receiver are separated by 1 km of fibre and a BSM node in between. The BSM and receiver share an entangled pair of photons emitted from the ELED. The input qubits interfere with biexciton photons on beamsplitter BS. Once detectors D1 and D2 measure their state, teleported output qubits are detected with a polarising beamsplitter (PBS) at D3 and D4. All state calibrations at each node are done with polarisation controllers (PCs). (**b**) Bell parameter extracted from experimental data. (**c**) Average third-order correlation $g^{(3)}$. Pulsed character of the correlations is observed. The single-photon property of emission is seen as a dip in coincidences at $\tau_2 = \tau_3$. Higher three-photon coincidences running along $\tau_2 = 0$ and $\tau_3 = 0$ originate from elevated probability of the ELED emitting a pair of photons simultaneously.

measured fidelity is the quantum bit error rate of the shared key. Error correction protocols are known that can correct for quantum bit error rate up to 0.2 in four-state protocols,[25] which corresponds to a minimum relay fidelity of 0.8, well below the experimentally measured value.

DISCUSSION

For smaller quantum bit error rate, as in our experiment, more effective error correction protocols are available.[26] Using the single photon, efficient BB84 protocol,[27] in the limit of infinitely many signals shared by the users, the fraction R of secure bits that can be extracted from each detected photon is[28]

$$R = 1 - h(Q_Z) - h(Q_X),$$

where h is the binary entropy function. By replacing the quantum bit error rates Q_Z and Q_X in the Z and X basis by those measured of 4.6% and 15.4% in the $\{H, V\}$ and $\{D, A\}$ bases, respectively, we find that 0.111 secure key bits can be distilled from our Relay per detected photon.

A key advantage of quantum-dot-based entangled light sources over spontaneous parametric downconversion is that they can in principle operate 'on-demand' and deterministically deliver a single entangled photon pair when triggered, without detrimental additional pairs. In our experiments, we measure the second-order correlation for coincident X photons to be close to optimal at 0.046 ± 0.008, highly suppressed from the Poissonian value of 1. Achieving maximal efficiency is predominantly limited by the photon collection efficiency, and the temporal post-selection window that heralds the occurrence of a teleportation event. Very high photon collection efficiencies have been reported in optically driven quantum dot nanostructures,[29,30] for which electrical injection schemes could be developed. Increasing the temporal region of high fidelity may be achieved by matching the laser and biexciton pulse shapes, reducing the excitation pulse width, reducing the fine-structure-splitting of 4.2 ± 0.1 μeV and extending the coherence time of the biexciton photons, which at 141.6 ± 4.2 ps limits the fidelity of teleporting D and A states.

In conclusion, we have reported the operation of a 203-MHz clocked quantum relay over 1 km of optical fibre using an electrically driven semiconductor light source. The measured relay fidelity of laser-generated photonic qubits of 0.900 ± 0.027 exceeds both the threshold for quantum behaviour, and the one for generating error-corrected quantum keys with the BB84 protocol. Coupled with advances of quantum-dot-based entangled light sources at telecom wavelengths, our results suggest ELED technology could meet the need for a practical solution to create the backbone of future quantum networks.

MATERIALS AND METHODS

Entangled light source

Entangled photon pairs are generated by an InAs quantum dot, embedded in a 2-lambda GaAs optical cavity within a p–i–n hetero-structure grown by molecular beam epitaxy. In order to improve light collection, 6 top and 18 bottom distributed Bragg reflectors pairs were

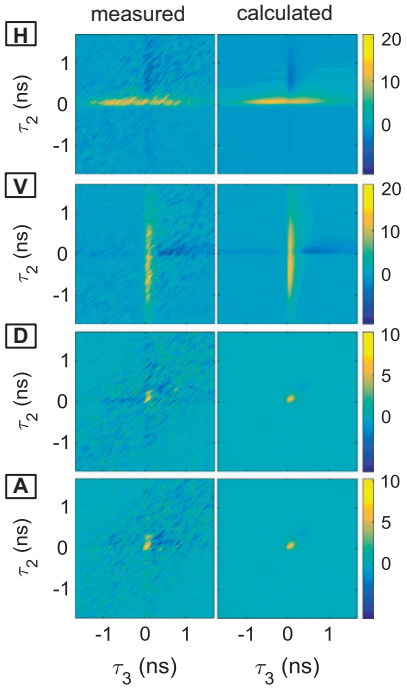

Figure 3. Polarisation dependence of third-order correlations. Difference between expected and unexpected third-order correlations $g^{(3)}$ as a function of photon detection time delays τ_2 and τ_3. Measured and calculated results are shown in the left and right column, respectively, corresponding to input states *H*, *V*, *D* and *A* (from top to bottom).

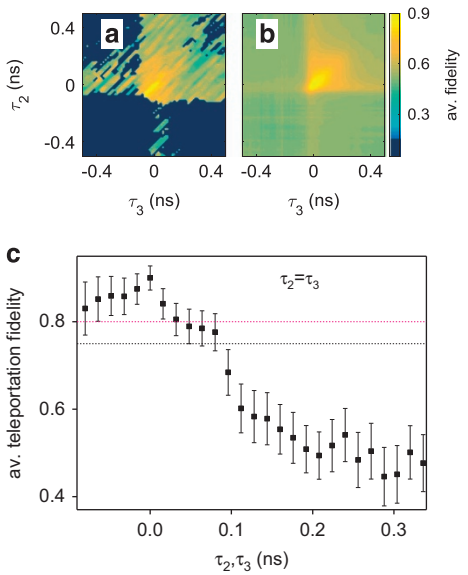

Figure 4. Quantum relay fidelity. (**a**, **b**) Relay fidelity averaged across four input qubit states *H*, *V*, *D* and *A*, as a function of the time delays τ_2 and τ_3. **a** and **b** shown experimental and simulated results, respectively. Note the measured fidelity is not defined in some regions of the plot as few photons were detected due to the ELED or laser being 'off' (dark blue). (**c**) Average relay fidelity as a function of time delay τ_2 and τ_3 for $\tau_2 = \tau_3$. High fidelity points are concentrated around $\tau_2, \tau_3 = 0$, where the measured fidelity exceeds the classical limit of 0.75 shown by black dashed line. The threshold for four-state error correction of 0.8 is shown as dashed red line.

grown. The relatively small dimensions of the mesa (210 × 110 μm) allow for a simple direct bonding design, while increasing the pulsed operation performance compared with previously reported, larger, ELEDs. The dot density is low enough so that no apertures were required and the light was collected using a single-mode fibre. The ELED device was driven by electrical injection at a frequency of 203 MHz, in forward bias, with a modulating alternating current voltage of nominally square pulses with 0.4 V amplitude and 490 ps width, at a temperature of 19.7 K. The emission spectrum of the dot under these conditions shows the biexciton *B* and exciton *X* at 885.7 and 887.3 nm, respectively. The fine-structure splitting was 4.2 ± 0.1 μeV. Higher operating frequency without sacrificing fidelity would be possible by optimising the voltage pulse profile across the intrinsic region, which otherwise causes the weak, long-lived tail in the electroluminescence shown in Figure 1d.

Quantum relay

For the input qubit photons at the sender section, a CW laser was externally modulated and synchronised with the dot driving frequency using a Mach–Zehnder optical intensity modulator. The generated pulses can have a full width at half maximum of 0.60 ± 0.02 ns. The relative time-integrated intensities between laser and biexciton photons incident on detectors D1 and D2 was set to 0.85:1. The input qubit polarisation state was selected using a pseudorandom number generator and polarisation controller PC1 at a frequency exceeding the three-photon coincidence rate. We note that the system is in principle compatible with quantum random number generators and phase modulation at frequencies exceeding the input qubit rate. The logical teleportation states {*H*, *V*} are calibrated to the quantum dot's polarisation eigenbasis, and the diagonal states {*D*, *A*} are set at ± 45° to the rectilinear basis using a linear polariser.

A 95:5 fibre beamsplitter was used to interfere the input laser photons with the biexciton photons. We only look at events from one output arm of this beamsplitter, which maximises the fraction of ELED photons detected in our experiment. The system was actively stabilised using electrical polarisation controllers at each of the sections during the experiment. The degree of polarisation for the input control qubits was maintained at 97.5 ± 1.5%. The 5% output port was used to spectrally tune the laser to the biexciton wavelength using a grating spectrometer, with an average detuning of 0.12 ± 1.68 μeV throughout the experiment.

Finally, photons at the BSM and receiver polarising beamsplitters were detected using four superconducting single-photon detectors with mean detection efficiency 31 ± 7%. The timing jitter between pairs of detectors was approximately Gaussian with full width at half maximum of 58.4 ± 2.5 ps, with single-photon-counting hardware resolution of 16 ps. The photon detection rate at the receiver was ~620 kHz, corresponding to an efficiency of ~0.3% per pulse after all losses, including long fibres.

Three-photon correlations

Three-photon coincidences were recorded corresponding to two photons at BSM detectors D1 and D2, with polarisation *H* and *V*, with one photon at either receiver's detectors D3 and D4. D3 and D4 record both expected photons with polarisation *P*′ and unexpected output photons with polarisation *Q*′ simultaneously.

The detection times at each detector are defined as t_1 (D1), t_2 (D2) and t_3 (D3 and D4). All events were recorded relative to detections at D1 (H-polarised photons). Third-order correlations $g^{(3)}$ for each output polarisation were determined from the normalised statistics of the three-photon coincidences, as a function of two time delays, $\tau_2 = t_3 - t_1$ and $\tau_3 = t_3 - t_2$. We note that the choice of which pair of time delays amongst the three photons to choose is somewhat arbitrary, for example, t_2–t_1 and t_3–t_1 have been used in previous reports. The three-photon detection rate was ~0.47 Hz, reduced to ~0.46 mHz for the strongest temporal post-selection window used here.

Error analysis

Errors are dominated by Poissonian counting statistics, which determines the errors on the third-order correlations from the number of photons detected. Errors are propagated to determine the relay fidelity errors of individual input states, and the average relay fidelity. Systematic errors due to the temporal calibration and resolution of our system are also included in the fidelity measurements, but are almost negligible. Note that all experimental three-photon results are presented for a time-integration

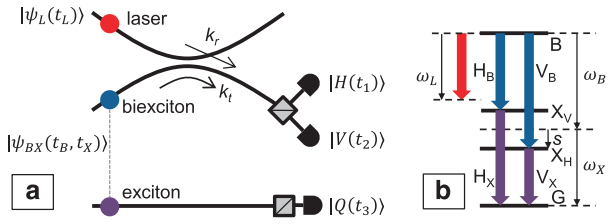

Figure 5. (**a**) Schematic of quantum relay scheme. Laser and biexciton photons meet at a fibre-optic coupler with transmission and coupling amplitudes k_t and k_r, before direction by a polarising beamsplitter to a pair of photon detectors. The exciton photon polarisation is selected in a given state *Q*, and measured by a third detector. (**b**) Level diagram showing the biexciton (*B*), exciton (*X*) and ground (*G*) states of a single quantum dot, plus the input laser photon. Frequencies and detunings of various photon states are shown.

window of 32 × 112 ps in τ_1 and τ_2, respectively, and evaluated on a 16-ps grid, so adjacent points are not independent.

Calculation of time-dependent $g^{(3)}$ correlations

In our experiments, we use a beamsplitter to combine laser photons with biexciton photons originating from an ELED, as shown in Figure 5a. To conserve biexciton photons from the entangled light source, the beamsplitter is highly imbalanced such that the transmission coefficient $|k_t| \gg |k_r|$. Only photons emerging on the efficient arm of the beamsplitter are measured, so for simplicity, the transmission and reflection coefficients of the beamsplitter, and phase change due to the coupling, are included within the amplitude and overall phase components of the laser and quantum dot wavefunction ψ_L and ψ_{BX}.

To begin, we define the laser and quantum dot states. In general, they are given by:

$$\psi_j = A_j(t_j)C_j(t_j)|\Psi_j(t_j)\rangle,$$

where $A_j(t_j)$ is the time-dependent real amplitude, $C_j(t_j)$ is the overall phase and $|\Psi_j(t_j)\rangle$ is the polarisation and any polarisation-dependent phase. The overall phase term is further defined as:

$$C_j(t_j) = e^{i\omega_j t_j} e^{i\phi_j(t_j)}.$$

The first exponent is coherent, and contributes to the final solutions only through detuning of ω_j to the primary frequencies ω_B and ω_X. Decoherence is represented by random fluctuations of the phase ϕ_j as a function of time t_j, such that $\langle e^{i[\phi_j(t_j)-\phi_j(t_j+\Delta)]}\rangle = e^{-|\Delta|/T_j}$, where T_j is the coherence time of photon *j*.[31,32]

For the laser input state with polarisation defined by real parameters *a* and *b*, we have

$$\psi_L = A_L(t_L)C_L(t_L)|\Psi_L\rangle,$$
$$|\Psi_L\rangle = \cos(a)|H\rangle + e^{ib}\sin(a)|V\rangle.$$

The output polarisation state is:

$$|\Psi_Q\rangle = \cos(x)|H\rangle + e^{iy}\sin(x)|V\rangle.$$

For photon pairs from the quantum dot, we have

$$\psi_{BX} = A_{BX}(t_B,t_X)C_B(t_B)C_X(t_X)|\Psi_{BX}(t_B,t_X)\rangle.$$

The ideal quantum dot biphoton amplitude and state are given by

$$A_{BXe}(t_B,t_X),$$
$$|\Psi_{BXe}\rangle = \left(e^{is(t_X-t_B)}|HH\rangle + e^{-is(t_X-t_B)}|VV\rangle\right)/\sqrt{2}.$$

In practice, however, the emission from the quantum dot is partially mixed. We approximate this with the amplitude $A_{BXu}(t_B, t_X)$ and equal mixture of the polarisation states:

$$\Psi_{HH} = e^{is(t_X-t_B)}|HH\rangle,$$
$$\Psi_{HV} = e^{is(-t_X-t_B)}|HV\rangle,$$
$$\Psi_{VH} = e^{is(t_X+t_B)}|VH\rangle,$$
$$\Psi_{VV} = e^{is(-t_X+t_B)}|VV\rangle.$$

The joint amplitude of the electric field at the three-photon detectors, *Z*, is given by the following equation, where four-photon contributions and higher are disregarded due to their relatively small probability compared with three-photon events:

$$Z(t_1,t_2,t_3) = \langle H|\psi_L(t_1)\rangle\langle VQ|\psi_{BX}(t_2,t_3)\rangle + \langle V|\psi_L(t_2)\rangle\langle HQ|\psi_{BX}(t_1,t_3)\rangle + \langle HV|\psi_{LL}(t_1,t_2)\rangle\langle Q|\psi_X(t_3)\rangle + \langle HVQ|\psi_{BBX}(t_1,t_2,t_3)\rangle.$$

The first two terms are the desired three-photon amplitudes originating from a single laser, biexciton and exciton photon. The third and fourth terms originate from two laser photons plus one exciton photon, and two biexciton photons plus one exciton photon, respectively.

The three-photon intensity $Z(t_1, t_2, t_3)Z^*(t_1, t_2, t_3)$ is evaluated and integrated over the arrival time of the *X* photon, t_3, from which we drop the subscript for convenience. Finally, we make substitutions of the form

$$\eta_j I_j(t_j) = A_j^2(t_j),$$
$$\eta_j\eta_k g_{jk}^{(2)}(t_j,t_k) = A_{jk}^2(t_j,t_k),$$
$$\eta_j\eta_k\eta_l g_{jkl}^{(3)}(t_j,t_k,t_l) = A_{jkl}^2(t_j,t_k,t_l).$$

where η_j is the time-averaged intensity of photon *j* and $I_j(t_j)$ the normalised intensity of photon *j* as a function of time. The final expression for the third-order correlation is:

$$\begin{aligned}
g^{(3)}(\tau_2,\tau_3) \propto\ & \frac{1}{2}\cos^2(a)\sin^2(x)\int_0^p I_L(t-\tau_2)g_{BXe}^{(2)}(t-\tau_3,t)\mathrm{d}t \\
& + \frac{1}{2}\sin^2(a)\cos^2(x)\int_0^p I_L(t-\tau_3)g_{BXe}^{(2)}(t-\tau_2,t)\mathrm{d}t \\
& + \frac{1}{4}\sin(2a)\sin(2x)e^{-\frac{|\tau_1|}{T_L}-\frac{|\tau_1|}{T_B}}\times\cos\left((\omega_B-\omega_L)\tau_1 - s(\tau_3+\tau_2)+y+b\right) \\
& \times\int_0^p\sqrt{(I_L(t-\tau_2)I_L(t-\tau_3)g_{BXe}^{(2)}(t-\tau_2,t)g_{BXe}^{(2)}(t-\tau_3,t)}\mathrm{d}t \\
& + \frac{1}{4}\cos^2(a)\int_0^p I_L(t-\tau_2)g_{BXu}^{(2)}(t-\tau_3,t)\mathrm{d}t \\
& + \frac{1}{4}\sin^2(a)\int_0^p I_L(t-\tau_3)g_{BXu}^{(2)}(t-\tau_2,t)\mathrm{d}t \\
& + \frac{\eta_L 1}{\eta_B 4}\cos^2(a)\sin^2(a)\int_0^p g_{LL}^{(2)}(t-\tau_2,t-\tau_3)I_X(t)\mathrm{d}t \\
& + \frac{\eta_B}{\eta_L}\int_0^p g_{BBX}^{(3)}(t-\tau_2,t-\tau_3,t)\mathrm{d}t.
\end{aligned}$$

Note the final term containing $g_{BBX}^{(3)}(t-\tau_2,t-\tau_3,t)$ is evaluated by substitution with chains of two-photon correlations, for different ordering of the two biexciton and one exciton photons. This is justified as detection of the first photon places the system to a well-defined state, which serves as the starting point for a correlation to a second photon, which after detection again places the system into another well-defined state, which is the starting point with correlation to a third photon. A factor of 1/2 in the penultimate term accounts for the Poissonian statistics of the laser two-photon intensity.

Optimum teleportation conditions

The single laser photon envelope I_L was approximated as a Gaussian function, which is a satisfactory approximation of what we observe in experiment. Single biexciton and exciton photon intensities $I_B(t_B)$ and $I_X(t_X)$ were directly measured, and the fine-structure-splitting and biexciton coherence time determined from polarisation-dependent spectroscopy and single-photon interferograms, respectively. Correlations were measured between biexciton and exciton photons to determine $g_{BX}^{(3)}(t_B, t_X - t_B)$ for co- and cross-linearly polarised states. The entangled and unentangled biphoton fractions $g_{BXe}^{(2)}$ and $g_{BXu}^{(2)}$ were extracted from half the difference between, and uncorrelated component of, these measurements, respectively. Similarly, correlations between pairs of biexciton photons $g_{BB}^{(2)}(t_1,t_2)$ were directly measured.

Note that imperfections in polarisation recovery and timing jitter are well represented in the parameter data, as the same physical measurement system was used for their measurement as for teleportation. However, additional jitter was added when evaluating the calculations to terms with discontinuities around zero delay. This fact, together with the lower time-averaged estimate of the coherence time compared with biexciton photons emitted in a single cycle, means that calculations are expected to underestimate the relay fidelity slightly, as observed.

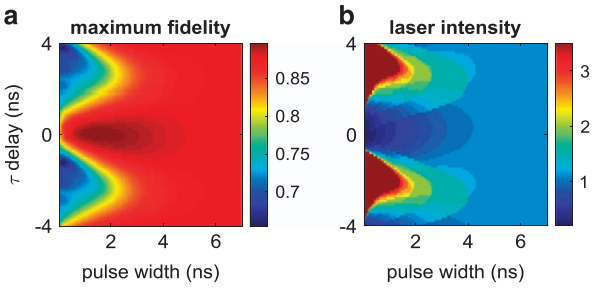

Figure 6. (**a**) Calculated maximum relay fidelity for our ELED with Gaussian laser pulses as a function of laser pulse width and delay relative to the biexciton photon. (**b**) Corresponding laser relative to biexciton intensity required (up to a limit of 3.5) to achieve maximal fidelity.

In order to maximise the relay fidelity in experiments, the expected maximal fidelity was calculated as a function of laser pulse intensity, width and delay relative to the biexciton photon. The results are summarised in Figure 6, which plots the calculated relay fidelity as a function of the pulse delay and width (Figure 6a), with corresponding optimal laser intensity (Figure 6b). Highest fidelities are observed for a laser delayed between −0.6 and 0.8 ns relative to maximal overlap with the biexciton state, and for a pulse width between 0.45 and 2.05 ns. The values used in our experiments are within this range.

Estimation of an upper bound to classical teleportation fidelity

The upper bound to classical teleportation fidelity in general depends on the set of possible input states. Following the methodology used to determine the upper bound for three[33] or six[21] input qubit states, the upper bound for which a BB84 compatible classical teleporter can operate is determined as follows.

In this experiment, Alice teleports four different qubits, equally spaced in the Poincaré sphere, in principle randomly selected with equal probability 1/4. This means that after many runs, Alice prepares the following statistical mixture:

$$\rho_{\text{in}} = |\Psi_{in}\rangle\langle\Psi_{in}| = \frac{1}{N}\sum_{n=1}^{N}|\Psi_n\rangle\langle\Psi_n|, \tag{1}$$

where $N=4$ and the $|\Psi_n\rangle$ are defined as:

$$|\Psi_1\rangle = |\uparrow\rangle, |\Psi_2\rangle = |\downarrow\rangle (\text{basis } Z)$$
$$|\Psi_3\rangle = \frac{1}{\sqrt{2}}(|\uparrow\rangle + |\downarrow\rangle), |\Psi_4\rangle = \frac{1}{\sqrt{2}}(|\uparrow\rangle - |\downarrow\rangle) (\text{basis } X)$$

These states are displaced at the four vertices of a square lying on the equator of the Poincaré sphere.

A 'classical teleportation protocol' is defined by the following procedure. Alice sends out one of the above states, $|\Psi_n\rangle$, chosen with equal probability 1/4. A user, called Charlie, measures the state as best as he can and then, based on the measurement's outcome, prepares a state $|\Psi_l^c\rangle$, which is as close as possible to the one he imagines to be $|\Psi_n\rangle$. The distance from the real one is measured by the classical fidelity F_c. Then Charlie sends the state $|\Psi_l^c\rangle$ to Bob, thus completing the transfer.

The best possible measure Charlie can do is a positive operator valued measurement. Let's then consider a non-orthogonal partition of the unity, done using L projectors (not necessarily orthonormal) $|\epsilon_l\rangle\langle\epsilon_l|$:

$$\sum_{l=1}^{L}|\epsilon_l\rangle\langle\epsilon_l| = I. \tag{2}$$

The states $|\epsilon_l\rangle$ compose an overcomplete set. Charlie receives $|\Psi_n\rangle$ and compares it with $|\epsilon_l\rangle$, thus obtaining a result l with probability $P_l = |\langle\Psi_n|\epsilon_l\rangle|^2$. With this information he prepares the pure state $|\Psi_l^c\rangle$ and sends it to Bob. After several measurements, the state prepared by Charlie is described by the mixture:

$$\rho_{\text{out}} = \sum_{l=1}^{L}P_l|\Psi_l^c\rangle\langle\Psi_l^c|. \tag{3}$$

So, using Equation (1), the obtained fidelity is

$$F_{c_{\text{POVM}}} = \frac{1}{N}\sum_{n=1}^{N}\sum_{l=1}^{L}|\langle\Psi_n|\epsilon_l\rangle|^2|\langle\Psi_n|\Psi_l^c\rangle|^2. \tag{4}$$

Now let us consider the normalised state $|\Omega_l\rangle$, with $|\epsilon_l\rangle = \sqrt{\mu_l}|\Omega_l\rangle$ and $\mu_l = \langle\epsilon_l|\epsilon_l\rangle$. Define:

$$T_l = \sum_{n=1}^{N}|\langle\Psi_n|\Omega_l\rangle|^2|\langle\Psi_n|\Psi_l^c\rangle|^2$$

so that

$$F_{c_{\text{POVM}}} = \frac{1}{N}\sum_{l=1}^{L}\mu_l T_l.$$

To calculate the maximum fidelity, we consider the following generic and independent two-dimensional states

$$|\Omega_l\rangle = \cos\frac{\alpha_l}{2}|\uparrow\rangle + e^{i\varphi_l}\sin\frac{\alpha_l}{2}|\downarrow\rangle$$
$$|\Psi_l^c\rangle = \cos\frac{\beta_l}{2}|\uparrow\rangle + e^{i\theta_l}\sin\frac{\beta_l}{2}|\downarrow\rangle$$

and calculate

$$\begin{aligned}T_l &= \sum_{n=1}^{4}|\langle\Psi_n|\Omega_l\rangle|^2|\langle\Psi_n|\Psi_l^c\rangle|^2\\ &= 2\cos^2\frac{\alpha_l}{2}\cos^2\frac{\beta_l}{2} - \cos^2\frac{\alpha_l}{2} - \cos^2\frac{\beta_l}{2}\\ &+ \frac{1}{2}\cos\theta_l\cos\varphi_l\sin\alpha_l\sin\beta_l\\ &+ \frac{3}{2}\leq 2\cos^2\frac{\alpha_l}{2}\cos^2\frac{\beta_l}{2} - \cos^2\frac{\alpha_l}{2} - \cos^2\frac{\beta_l}{2} + \frac{1}{2}\sin\alpha_l\sin\beta_l + \frac{3}{2}\\ &= \frac{1}{2}\cos(\alpha_l - \beta_l) + 1 \leq \frac{3}{2}\end{aligned} \tag{5}$$

Using Equations (2) and (5) we finally have

$$\begin{aligned}F_{c_{\text{POVM}}} &= \frac{1}{4}\sum_{l=1}^{L}\mu_l T_l \leq \frac{1}{4}\sum_{l=1}^{L}\mu_l \times \frac{3}{2} = \frac{3}{8}\sum_{l=1}^{L}\mu_l\\ &= \frac{3}{8}tr\sum_{l=1}^{L}|\epsilon_l\rangle\langle\epsilon_l| = \frac{3}{8}trI = \frac{3}{8}\times 2 = \frac{3}{4}.\end{aligned}$$

ACKNOWLEDGEMENTS

The authors thank M Razavi for theoretical support and C Panayi for useful discussions. The data from this paper are available at https://www.repository.cam.ac.uk/handle/1810/253299. The authors acknowledge partial financial support through the UK EPSRC and the EU Marie Curie Initial Training Network Spin-optronics.

CONTRIBUTIONS

Samples were grown by IF and DAR and processed by JS-S and CV; optical experiments were performed by CV and RMS, with contributions from JN and BD; theory for correlations was developed by RMS, JN and CV, and theory for security by ML, RMS and BD; RVP supervised CV; AJS guided the work; all authors discussed the experiments, results and their interpretation; RMS and CV wrote the manuscript, with contributions from the other authors.

COMPETING INTERESTS

The authors declare no conflict of interest.

REFERENCES

1. Gisin, N., Ribordy, G., Tittel, W. & Zbinden, H. Quantum cryptography. *Rev. Mod. Phys.* **74**, 145–195 (2002).
2. Scarani, V. *et al.* The security of practical quantum key distribution. *Rev. Mod. Phys.* **81**, 1301–1350 (2009).
3. Rosenberg, D. *et al.* Long-distance decoy-state quantum key distribution in optical fiber. *Phys. Rev. Lett.* **98**, 010503 (2007).
4. Dixon, A. R., Yuan, Z. L., Dynes, J. F., Sharpe, A. W. & Shields, A. J. Continuous operation of high bit rate quantum key distribution. *Appl. Phys. Lett.* **96**, 161102 (2010).
5. Wang, S. *et al.* 2-GHz clock quantum key distribution over 260 km of standard telecom fiber. *Opt. Lett.* **37**, 1008–1010 (2012).
6. Fröhlich, B. *et al.* A quantum access network. *Nature* **501**, 69–73 (2013).
7. Peev, M. *et al.* The SECOQC quantum key distribution network in Vienna. *New J. Phys.* **11**, 075001 (2009).
8. Jacobs, B. C., Pittman, T. B. & Franson, J. D. Quantum relays and noise suppression using linear optics. *Phys. Rev. A* **66**, 052307 (2002).
9. Ekert, A. K. Quantum cryptography based on Bell's theorem. *Phys. Rev. Lett.* **67**, 661–663 (1991).
10. Braunstein, S. L. & Pirandola, S. Side-channel-free quantum key distribution. *Phys. Rev. Lett.* **108**, 130502 (2012).
11. Lo, H.-K., Curty, M. & Qi, B. Measurement-device-independent quantum key distribution. *Phys. Rev. Lett.* **108**, 130503 (2012).
12. Tang, Y.-L. *et al.* Measurement-device-independent quantum key distribution over 200 km. *Phys. Rev. Lett.* **113**, 190501 (2014).
13. Briegel, H.-J., Dür, W., Cirac, J. I. & Zoller, P. Quantum repeaters: the role of imperfect local operations in quantum communication. *Phys. Rev. Lett.* **81**, 5932–5935 (1998).
14. de Riedmatten, H. *et al.* Long distance quantum teleportation in a quantum relay configuration. *Phys. Rev. Lett.* **92**, 047904 (2004).
15. Ma, X.-S. *et al.* Quantum teleportation over 143 kilometres using active feed-forward. *Nature* **489**, 269–273 (2012).
16. Bussières, F. *et al.* Quantum teleportation from a telecom-wavelength photon to a solid-state quantum memory. *Nat. Photon.* **8**, 775–778 (2014).
17. Brassard, G., Lütkenhaus, N., Mor, T. & Sanders, B. C. Limitations on practical quantum cryptography. *Phys. Rev. Lett.* **85**, 1330–1333 (2000).
18. Stevenson, R. M. *et al.* Quantum teleportation of laser-generated photons with an entangled-light-emitting diode. *Nat. Commun.* **4**, 2859 (2013).
19. Lo, H.-K. & Chau, H. F. Unconditional security of quantum key distribution over arbitrarily long distances. *Science* **283**, 2050–2056 (1999).
20. Salter, C. L. *et al.* An entangled-light-emitting diode. *Nature* **465**, 594–597 (2010).
21. Nilsson, J. *et al.* Quantum teleportation using a light-emitting diode. *Nat. Photon.* **7**, 311–315 (2013).
22. Bennett, C. H. *et al.* Teleporting an unknown quantum state via dual classical and Einstein-Podolsky-Rosen channels. *Phys. Rev. Lett.* **70**, 1895–1899 (1993).
23. Young, R. J. *et al.* Bell-inequality violation with a triggered photon-pair source. *Phys. Rev. Lett.* **102**, 30406 (2009).
24. Bennett, C. H., Brassard, G. In *Proc. IEEE International Conference on Computers, Systems and Signal Processing, Bangalore, India*. 175–179 (IEEE, New York, NY, USA, 1984).
25. Chau, H. F. Practical scheme to share a secret key through a quantum channel with a 27.6% bit error rate. *Phys. Rev. A* **66**, 060302(R) (2002).
26. Brassard, G, Salvail, L. in *Advances in Cryptology—EUROCRYPT '93: Lecture Notes in Computer Science* Vol. 765 (ed. Helleseth, T.) 410–423 (Springer, 1994).
27. Lo, H.-K., Chau, H. F. & Ardehali, M. Efficient quantum key distribution scheme and proof of its unconditional security. *J. Cryptology* **18**, 133–165 (2005).
28. Koashi, M. Simple security proof of quantum key distribution based on complementarity. *New J. Phys.* **11**, 045018 (2009).
29. Dousse, A. *et al.* Ultrabright source of entangled photon pairs. *Nature* **466**, 217–220 (2010).
30. Claudon, J. *et al.* A highly efficient single-photon source based on a quantum dot in a photonic nanowire. *Nat. Photon.* **4**, 174–177 (2010).
31. Legero, T., Wilk, T., Kuhn, A. & Rempe, G. Time-resolved two-photon quantum interference. *Appl. Phys. B* **77**, 797–802 (2003).
32. Santori, C., Fattal, D., Vuckovic, J., Solomon, G. S. & Yamamoto, Y. Single-photon generation with InAs quantum dots. *New J. Phys.* **6**, 89 (2004).
33. Boschi, D., Branca, S., De Martini, F., Hardy, L. & Popescu, S. Experimental realization of teleporting an unknown pure quantum state via dual classical and Einstein-Podolsky-Rosen channels. *Phys. Rev. Lett.* **80**, 1121–1125 (1998).